Analysis of Resonant Current Influence on Capacitor Lifetime Variation in LCL-Type Photovoltaic Systems

Jiacheng Sun, *Graduate Student Member, IEEE*, Xinyue Zhang, *Member, IEEE*, Wenli Yao, *Member, IEEE*, Xiaobin Zhang, and Dao Zhou, *Senior Member, IEEE*

***Abstract*—Ensuring reliability is vital for the efficient operation, maintenance, and cost-effectiveness of LCL-type photovoltaic (PV) inverters. The resonant currents triggered by the filter may transmit and couple between the grid and the PV system, thereby amplifying the electrothermal stresses on capacitors and resulting in notable inaccuracies in lifetime predictions. This article thoroughly analyzes capacitor lifetime to quantify estimation errors arising from resonant currents. Differing from conventional analysis, the electrical stresses with resonances are obtained by Fourier series and impedance characteristics of the LCL filter. This method ensures that the model analysis remains independent of simulations, making it easy to modify and optimize. Furthermore, the capacitor's electrical stresses are validated experimentally. The findings indicate that resonant current significantly reduces capacitor lifetime. The damping method's failure leads to a 24% reduction in the capacitor bank's lifetime, with a notable 60% decrease observed particularly when utilizing a 15 μF individual capacitor. Ultimately, the comparison of average lifetime costs among various capacitor banks is conducted based on the proposed analytical model and reliability estimation method, aiming to optimize economic performance from a reliability perspective. The results of the lifetime investigation provide further insights into the LCL-type PV system design.**

***Index Terms*—Film capacitors, LCL filter, reliability evaluation, resonant current.**

I. Introduction

With the increasing penetration of renewable energy generation systems, inverters have evolved into efficient grid interfaces. LCL filters are commonly utilized in power generation systems to filter out switching harmonics. Compared with single inductor filters, it can achieve higher harmonic attenuation with less component weight [1].

Received 30 March 2024; revised 23 July 2024; accepted 31 August 2024. Date of publication 11 September 2024; date of current version 7 October 2024. This work was supported by the National Natural Science Foundation of China under Grant 52007154. Recommended for publication by Associate Editor M. Liserre. *(Corresponding author: Wenli Yao.)*

Jiacheng Sun, Xinyue Zhang, Wenli Yao, and Xiaobin Zhang are with the School of Automation, Northwestern Polytechnical University, Xi'an 710072, China (e-mail: sunakon@mail.nwpu.edu.cn; zhang_xin_yue@mail.nwpu.edu.cn; yaowl@nwpu.edu.cn; zxb907@nwpu.edu.cn).

Dao Zhou is with the Department of Energy, Aalborg University, 9220 Aalborg, Denmark (e-mail: zda@et.aau.dk).

Color versions of one or more figures in this article are available at https://doi.org/10.1109/TPEL.2024.3457828.

Digital Object Identifier 10.1109/TPEL.2024.3457828

In renewable energy sources, such as photovoltaic (PV), the high maintenance costs have emphasized the increasing importance of power electronic system reliability [2]. Capacitors are among the most vulnerable components [3], metalized polypropylene film capacitors (MPF-CAPs) are normally applied in LCL filter on the ac side [4]. However, recent literature has predominantly concentrated on methods to evaluate the lifetime of aluminum electrolytic capacitors on the dc side [3], [4], [5]. Typically, capacitor manufacturers provide models that predict the lifetime of their products, considering particular conditions, such as ambient temperature, ripple current, applied voltage, and core temperature [6], [7]. Nonetheless, relying on this model may not accurately reflect the lifetime of capacitors in the real-world operation [8]. To enhance reliability accuracy, a majority of literature has investigated reliability analysis based on the mission profiles. In [9] and [10], a real mission profile is used to evaluate the reliability of capacitors. However, research focusing on the reliability of LCL filter capacitors is lacking.

Employing LCL filters in PV can potentially compromise the system's reliability, leading to higher maintenance expenses. LCL filter as a third-order system, generated resonant peaks may challenge the stability of the system depending on the time delay and current control scheme [11]. Passive damping and active damping are commonly applied to suppress the resonant current [12]. However, some damping methods are sensitive to parameter variations and uncertainties [13], making the stability of the system vulnerable to slight parameter drifts. Even in a critical condition, long-term resonance poses a potential risk to component reliability [14]. Similarly, in a weak grid scenario, the grid impedance and the LCL resonance frequency may vary widely, leading to oscillations within the system [15]. It should be noted that even with the implementation of the abovementioned damping methods, nonideal factors, such as time delay, grid background harmonics, grid fault, and variations in grid impedance can still significantly impact the performance and stability of the grid-connected inverter system in practical digital control [16]. Therefore, this article focuses on quantitatively analyzing the impact of resonant currents on capacitor lifetime when the system oscillates.

However, recent power quality issues have indicated that unbalanced voltages caused by grid faults are the most common type of disturbance [17]. In [18], the effect of grid unbalance on the lifetime of dc-link capacitors is discussed, but the lifetime

analysis is limited to electrolytic capacitors. In [19], the harmonic spectrum of electrical stresses on capacitor current under modulation techniques and grid conditions is investigated, where only simulation results are presented. The current spectrum is calculated in [3] and [20] using complicated double Fourier analysis, which however ignores an important concern, the effect of resonant current of LCL filters on thermal stress and lifetime of capacitors. However, studies of LCL filters focus on internal stability [21] and external stability [22], the resonant currents triggered by the filter may transmit and couple between the grid and the PV system. The existing research neglects to address the impact of resonance-induced electrical stresses on capacitor lifetime. In [23], the impact of electrical stresses by reactive power on capacitor aging is considered, but the impact is limited and mainly focused on parameter shift in equivalent series resistance (ESR).

The lifetime of capacitor is determined by several parameters. Some researchers have investigated the ESR and capacitance variation of capacitors [5]. With increasing ESR, the capacitance value decreases, which in turn impacts the capacitor's lifetime [24]. Meanwhile, unbalanced voltage and background harmonics significantly influence the electrothermal stresses of the capacitor [23]. The resonant current caused by the LCL filter can lead to internal self-heating and thus increase the hotspot temperature, which accelerates the aging process of the filter capacitor. In order to fill up the research gap regarding the impacts of resonant current on capacitor reliability, this article proposes an analytical method for assessing its influence on the lifetime of LCL filter capacitors. In particular, the Fourier series is employed to analyze harmonic voltage, whereas the characteristics of the filter impedance are employed to evaluate the electrical stresses of the capacitor current. A thermal model, based on the mission profile, is established to predict the lifetime of an individual capacitor. In renewable energy applications, multiple capacitors are typically connected in series or parallel. However, the component-level B_{10} lifetime of a single capacitor cannot be directly translated into the system-level B_{10} lifetime of a capacitor bank (B_{10} lifetime is percentile lifetime, defined as the 10% failure of a sample when the operating time reaches the designed lifetime). In this article, the Weibull distribution will be fitted using Monte Carlo simulation, considering the uncertainty of parameters. In addition, the reliability block diagram is employed to convert the lifetime of a single capacitor into the lifetime of a capacitor bank.

Subsequently, a cost comparison is presented for different capacitor banks with a consistent total capacitance value, which provides a performance reference for the capacitor bank selection. Compared with the traditional reliability assessment, some improvements are made, given as follows.

1) A model based on the Fourier transform is constructed to analyze the electrical stress distribution of capacitor currents that exhibit resonances. They ensure that evaluations of electrical stress and power loss are not only independent of the simulation analysis but also free from the constraints of the filter parameters.
2) This article presents a quantitative assessment and comparison of the damage inflicted by resonant currents on capacitors. By considering reliability, it offers a novel perspective on designing LCL-type PV converters. Recommendations for cost-effective capacitor banks are also provided to optimize cost and reliability.

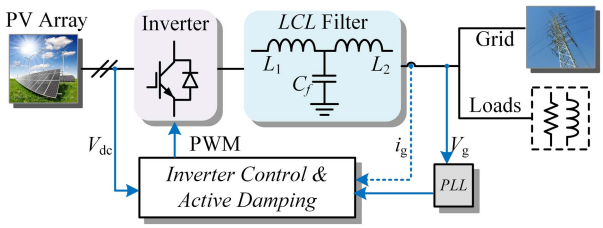

Fig. 1. System configuration and control structure of PV system.

TABLE I
PARAMETERS OF THE SYSTEM

Parameters	Values
Converter-side inductor	L_1 = 1.8 mH
Grid-side inductor	L_2 = 2 mH
Filter capacitor	C_f = 15 μF
Grid voltage	V_g = 220 V/50 Hz
DC voltage	V_{dc} = 360 V
Sample frequency	f_s = 10 kHz
Switching frequency	f_{sw} = 10 kHz
Output power	P_o = 2.6 kW
Resonance frequency	f_{res} = 1336 Hz (27^{th} Har.)

The rest of this article is organized as follows. Section II describes the basic design of a home PV inverter based on the mission profile, and Section III presents the analysis of capacitor resonant current with calculations and simulations. Section IV shows the experimental validation of the electrical stress analysis of the capacitor current. Section V evaluates the lifetime of single capacitor and capacitor banks and uses reliability block diagrams to compare the significant effect of the capacitor lifetime with and without resonant currents. Finally, Section VI concludes this article.

II. Case Study Description

A. System Description

The configuration and control structure of a smart home/building with a single-phase PV system is shown in Fig. 1, and the parameters are given in Table I. It can be seen that a full-bridge inverter is utilized as an efficient grid interface. Besides, an LCL filter is employed to eliminate the higher order harmonics caused by pulsewidth modulation (PWM) [12]. However, due to the inherent resonance characteristics of LCL filters, mitigating oscillations to achieve system stability is crucial. Typical current controllers employ state-of-the-art damping controls (e.g., capacitor current feedback [25] and grid voltage feedforward [17]) to ensure system stability under various conditions, such as grid faults. The current controller in Fig. 1 is implemented by controlling the grid current i_g, while a phase-locked loop is implemented for synchronization [1]. Despite applying damping control, the system can still experience critical

oscillations during passive component parameter drift or grid impedance variation due to the limited robustness of the current controller. These oscillations inevitably affect the reliability of the filter capacitors. It is worth noting that the various causes of system oscillations are beyond the scope of this article, which aims to provide a guideline for evaluating capacitor lifetime errors caused by resonant currents.

B. Design of Filter Capacitors

The LCL filter is designed to reduce high-order harmonics on the grid-side. However, a poorly designed filter can result in less attenuation than expected, or even increase distortion due to oscillation effects. To enhance the overall integrality and readability of this article, the LCL filter capacitor selection program follows the design procedure recommendations in [11], using the converter's power rating and line frequency as inputs. In the following development, the filter values are reported as a percentage of the base values, defined as follows:

$$Z_0 = \frac{V_g^2}{P_0} \tag{1}$$

$$C_0 = \frac{1}{\omega_g Z_0} \tag{2}$$

where V_g is the grid voltage, ω_g is the grid frequency, and P_0 is the rated power. However, the filter capacitor C_f introduces reactive power. Greater capacitance generates more reactive power, which increases current through the power device and leads to higher conduction losses [23]. Typically, the reactive power generated by the filter capacitor should be less than 10% of the rated power. Therefore, the capacitor value can be expressed as a percentage as follows:

$$C_f < 10\% C_0. \tag{3}$$

In this case, three capacitor configurations are utilized, optimizing cost and size from the film capacitor manufacturer [26]. The total capacitance is held constant at 15 μF, achieved through a single 15 μF capacitor, three 5 μF in parallel, or five 3 μF in parallel. This design maintains a consistent resonant frequency for the system.

C. Mission Profile of the PV Systems

The mission profiles from the PV geographical information system in Fig. 2 are applied to the electrothermal model. Solar irradiance (SI) and ambient temperature are two parameters that are highly relevant for the mission profile of PV systems. It should be noted that in actual installation scenarios, the ambient temperature of a single-phase PV system may differ from the applied temperature of the mission profile. In the case that the degradation of the PV panels is ignored [27]. The generated power can be predicted from the maximum power point tracking curve and the SI [28]. Furthermore, the capacitor current and voltage stresses can be evaluated based on the PV system model.

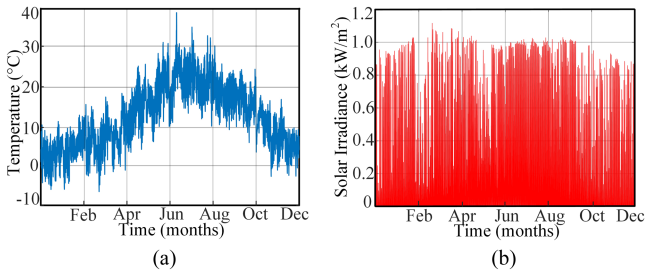

Fig. 2. One-year mission profiles. (a) Ambient temperature. (b) Solar irradiance.

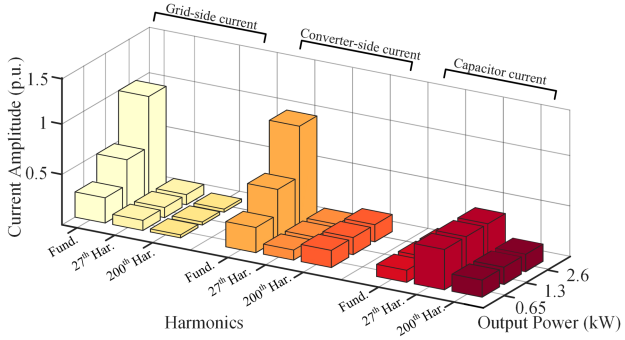

Fig. 3. Harmonic comparison of grid-side current, converter-side current, and capacitor current at different powers.

III. Electrical Stresses Analysis of Capacitors

The SI directly influences the output power of a single-phase PV inverter system designed for smart homes/buildings. Consequently, comparisons are made among the fundamental component, resonant harmonic component (27th), and switching harmonic component (200th) of the current under different output power conditions. As shown in Fig. 3, when the resonant current is present, the simulated fundamental component of the grid-side current at rated power remains at 1.0 per unit (p.u.). Given that the LCL filter typically acts as a low-pass filter, the fundamental components of the grid-side current and the converter-side current are nearly identical at the same output power level. However, they exhibit significant variations when the output power levels differ. Furthermore, the harmonic components, resulting from modulation, show minimal changes at different output powers, leading to similar harmonic components in the converter-side and grid-side currents across various power levels. Notably, the switching harmonics of the grid-side current are considerably reduced compared with the converter-side current because most of the switching harmonics flow through the filter capacitor. It is worth mentioning that the p.u. values of the fundamental and harmonic components of the capacitor current in the simulation hardly fluctuate with the variation of the output powers.

Resonant currents induce internal self-heating, raising hotspot temperature, thus accelerating to capacitor aging, which is a key factor of failure. To assess the reliability of capacitors, it is useful to quantitatively compare the differences in capacitor power loss

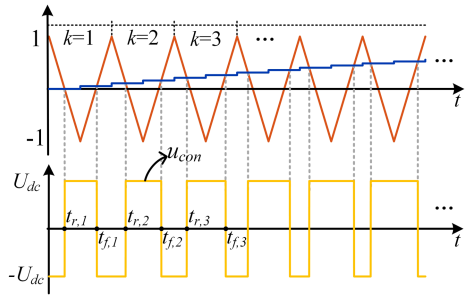

Fig. 4. Principle of asymmetrically sampled PWM process.

under different electrical stresses. It is known that the power loss is related to the current amplitude. Therefore, ensuring accurate calculations of electrical parameters is crucial for evaluating their reliability. However, achieving precise calculations can be challenging, particularly under oscillating conditions. Typically, in converters, obtaining capacitor current involves analytical simulations models, and experimental measurements [29]. However, when the resonant current demonstrates a nonpure sinusoidal state with high-frequency harmonics. These approaches encounter challenges in simple modification and optimization due to a notable increase in complexity. In this article, a single-phase inverter employing bipolar sinusoidal PWM is utilized, and a single Fourier series is applied to determine the amplitude of the inverter's output voltage for various harmonic orders. Then, according to the impedance characteristics of the LCL filter, the corresponding capacitor current amplitude can be calculated, thus establishing independence from simulation analysis in capacitor stress assessment. The Fourier coefficients for a periodic voltage waveform can be calculated using the switching angle's time period and amplitude [30]. Fig. 4 shows the PWM process when applying asymmetrical regular sampling. The points of intersection between the modulating and carrier waves correspond to the rising edge instant $t_{r,k}$ and the falling edge instant $t_{f,k}$ of the converter output voltage $u_{\text{con}}(t)$, as shown in (4) and (5), respectively. Both contain the fundamental part and the resonant part. Then, $u_{\text{con}}(t)$ can be denoted as (6)

$$t_{r,k} = \frac{\pi}{2\omega_c}\left(4k - 3 + \underbrace{M_0 \sin\frac{(2k-2)\pi}{N}}_{\text{Fundamental part}} + \underbrace{M_n \sin n\frac{(2k-2)\pi}{N}}_{\text{Resonant part}}\right) \tag{4}$$

$$t_{f,k} = \frac{\pi}{2\omega_c}\left(4k - 1 - \underbrace{M_0 \sin\frac{(2k-1)\pi}{N}}_{\text{Fundamental part}} - \underbrace{M_n \sin n\frac{(2k-1)\pi}{N}}_{\text{Resonant part}}\right) \tag{5}$$

$$u_{\text{con}}(t) = \begin{cases} U_{\text{dc}}, & t_{r,k} < t < t_{f,k} \\ -U_{\text{dc}}, & \text{else} \end{cases} \tag{6}$$

where the variables $k = 1, 2, 3.....$ defines the index of the carrier period. n and U_{dc} represent the harmonic order and dc input voltage, respectively. $N = \omega_c/\omega_0$ is the carrier ratio, ω_c is the angular frequency of the carrier wave, and ω_0 is the angle frequency of the modulation signal. In addition, M_n represents the amplitude modulation index at the nth harmonic. The modulation index of the converter voltage can be deduced from the converter system modeling. According to Dirichlet Theorem [30], [31], the single Fourier series [32] of voltage $u_{\text{con}}(t)$ is given as follows:

$$u_{\text{con}}(t) = \frac{a_0}{2} + \sum_{n=1}^{\infty}(a_n \cos n\omega_0 t + b_n \sin n\omega_0 t) \tag{7}$$

where the first term in (7), $a_0/2$ denotes the dc offset of the converter output voltage and the coefficients a_n and b_n can be derived as follows:

$$\begin{cases} a_n = \frac{2U_{\text{dc}}}{n\pi}\sum_{k=1}^{N}\left[\sin(n\omega_0 t_{f,k}) - \sin(n\omega_0 t_{r,k})\right] \\ b_n = -\frac{2U_{\text{dc}}}{n\pi}\sum_{k=1}^{N}\left[\cos(n\omega_0 t_{f,k}) - \cos(n\omega_0 t_{r,k})\right]. \end{cases} \tag{8}$$

Then, the plural form m_n of two coefficients a_n and b_n can also be expressed as $m_n = a_n + jb_n$. The voltage amplitude $|m_n|$ of the nth-order harmonic can be obtained as follows:

$$|m_n| = \sqrt{a_n^2 + b_n^2} \tag{9}$$

A detailed expression (10) for the harmonic order contained in $|m_n|$ is shown at the bottom of the next page. According to the above Fourier Series decomposition, the amplitude of the converter output voltage can be calculated using the parameters in Table I. It is important to emphasize that the Fourier series discussed in this article is specifically applicable to common two-level grid-connected inverters. The relationship between the converter output voltage and the electrical stresses on the filter capacitor is closely dependent on the characteristics of the LCL filter. As shown in Fig. 5, it can be seen that the capacitor current will be significantly amplified at the resonant frequency. By referencing the impedance characteristics of the LCL filter depicted in (11), it becomes feasible to compute the filter capacitor currents, both with and without resonant current. The calculation results are shown in Fig. 6

$$Z_{LCL-c}(s) = \frac{u_{\text{con}}(s)}{i_c(s)} = \frac{L_1 L_2 C_f s^3 + (L_1 + L_2)s}{L_2 C_f s^2}. \tag{11}$$

Utilizing the harmonic spectrum of the capacitor current, the total harmonic distortion (THD) can be obtained. At rated power, the voltage harmonics in Fig. 6(a) are primarily influenced by the switching frequency and its multiples. Notably, under conditions of system oscillation, significant components around the 27th voltage harmonic are observed. The capacitor current exhibits a similar harmonic trend at the switching frequency as the voltage harmonics, in the presence of resonant current. In addition, it is also worth noting that due to the impedance characteristics of the LCL filter, the 27th current harmonic is significantly amplified, while the fundamental current is reduced considerably, resulting

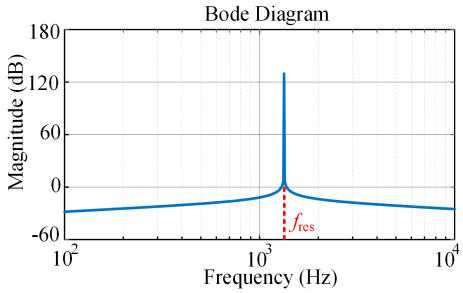

Fig. 5. LCL filter characteristic from converter output voltage to filter capacitor current.

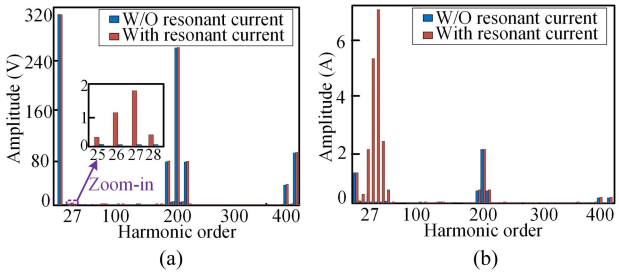

Fig. 6. FFT analysis of calculated results in the inverter system. (a) Converter output voltages. (b) Capacitor currents.

in a THD of 677% for the capacitor current. When the damping method is applied, as shown in Fig. 6(b), the capacitor current mainly contains the fundamental and switching harmonics, resulting in a THD of 168%. This increase in THD signifies an elevation in the electrical stresses on the capacitor when the damping method fails.

To confirm the viability of the above capacitor current model, the commercial simulation tool PLECS is employed. Fig. 7 shows the simulation results of the inverter system, investigating the harmonic spectrum of the output voltage and the filter capacitor current with and without resonant currents. Concerning the converter output voltage, the fundamental components and switching harmonics are in close match with the theoretical calculations. In the case of capacitor current, Fig. 7(a) illustrates that it primarily comprises switching and resonant harmonics when the system resonates, resulting in a THD of 682%. However, as depicted in Fig. 7(b) when the damping method is applied it contains only switching harmonics and the THD of the capacitor current is 172%. These simulation results demonstrate a close agreement with theoretical calculations. It is important to highlight that, unlike the typical evaluation of electrical stresses, this article characterizes the capacitor currents with resonant distributions using Fourier series. This approach ensures that the electrical stress model is independent of simulation analysis,

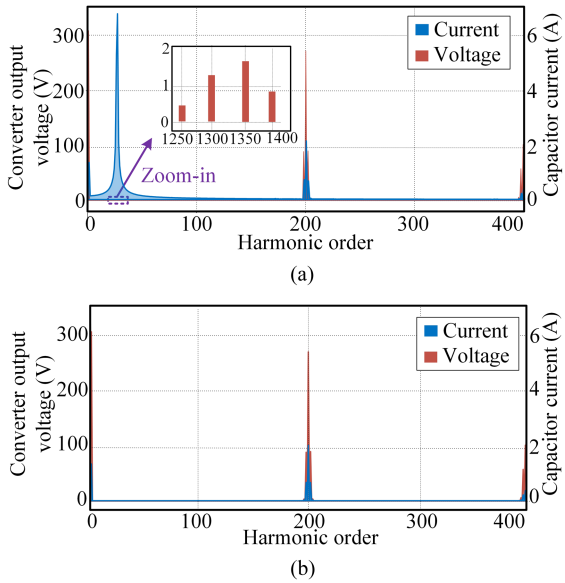

Fig. 7. FFT analysis of simulation results in the inverter system. (a) Converter output voltage and capacitor current with resonant current. (b) Converter output voltage and capacitor current without resonant current.

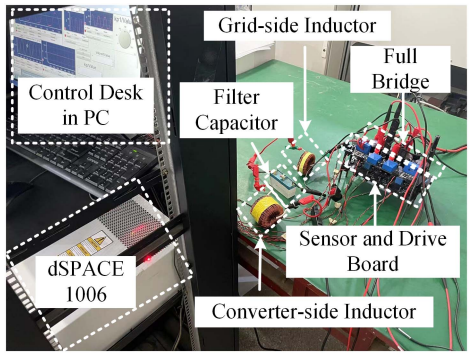

Fig. 8. Experimental prototype of a single-phase LCL-filtered converter.

allowing it to be applied to other applications with LCL filters. Furthermore, it is not constrained by the number of resonant orders, facilitating easier modification and optimization.

IV. Capacitor Current Measurement in Experiments

In order to assess the variations in electrical stress on capacitors due to the presence or absence of resonant currents, a prototype single-phase LCL filter converter is developed, as depicted in Fig. 8, with its parameters detailed in Table I. The converter-side inductor L_1 is designed according to a peak-to-peak current ripple [33], which is chosen to be 1.8 mH due to laboratory limitations. Similarly, the grid-side inductor L_2 is

$$|m_n| = \frac{2U_{\rm dc}}{n\pi}\sqrt{\sum_{i=1}^{N}\sum_{j=1}^{N}\left[\cos(n\omega_0 t_{f,i} - n\omega_0 t_{f,j}) - \cos(n\omega_0 t_{f,j} - n\omega_0 t_{r,i}) - \cos(n\omega_0 t_{f,i} - n\omega_0 t_{r,j}) + \cos(n\omega_0 t_{r,i} - n\omega_0 t_{r,j})\right]}. \tag{10}$$

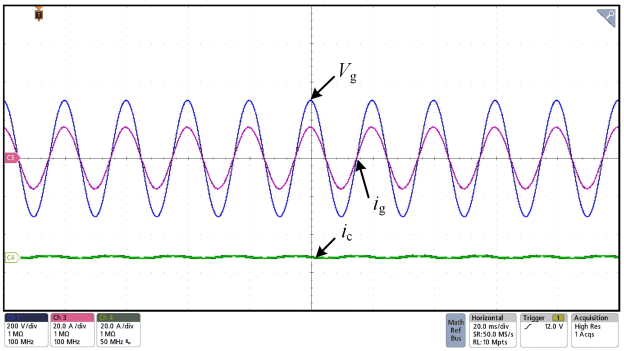

Fig. 9. Experimental results of single-phase LCL-filtered converter during system stabilization. (grid current i_g: 20 A/div, grid voltage V_g: 200 V/div, capacitor current i_c: 20 A/div, and time: 20 ms/div.).

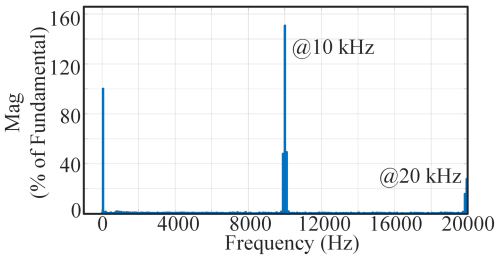

Fig. 10. FFT analysis results of capacitor current during system stabilization.

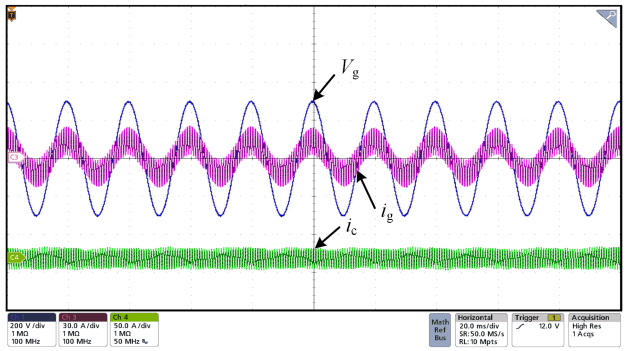

Fig. 11. Experimental results of single-phase LCL-filtered converter during system oscillations. (grid current i_g: 30 A/div, grid voltage V_g: 200 V/div, capacitor current i_c: 50 A/div, and time: 20 ms/div).

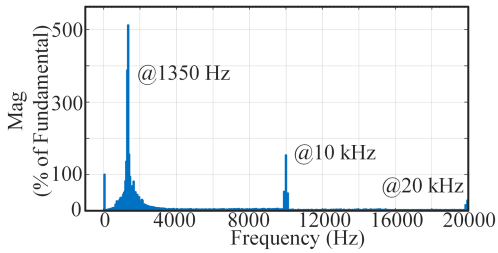

Fig. 12. FFT analysis results of capacitor current during system oscillations.

chosen with a 2 mH value to further reduce the peak-to-peak current ripple. The control scheme of the power converter is realized by dSPACE 1006 with the switching frequency of 10 kHz. It is worth noting that both stabilization and oscillation modes are employed in order to investigate the impact of the resonant current on the electrical stresses in the capacitors. The grid voltages and currents are measured to observe the operation condition of the converter, and the currents flowing through the filter capacitors are also measured to evaluate the variations in the electrical stresses. From Fig. 9, it can be seen that the stability of the system is ensured due to the damping method that suppresses the resonances of the LCL filter. With a switching frequency of 10 kHz, the switching harmonics of the capacitor currents become prominent during system stabilization. These harmonics of the capacitor current fast fourier transform (FFT) analysis results are approximately at 10 and 20 kHz, as illustrated in Fig. 10, with a THD of 175%, which are in good agreement with the simulation results in Fig. 7(b).

Fig. 11 shows the experimental waveforms of the critical oscillations within the system when the damping method fails, clearly illustrating oscillations in both the grid current and the filter capacitor current. The capacitor current FFT analysis is shown in Fig. 12, which reveals the dominance of the 27^{th} current harmonic, followed by the switching harmonics at 10 and 20 kHz, with a THD of 686%, consistent with the simulation FFT analysis results in Fig. 7(a). In addition, due to the impedance characteristics of the LCL filter, the 27th current harmonic amplitude is significantly amplified and much larger than the amplitudes of the switching harmonics and the fundamental, which is consistent with the theoretical analysis results in Section III. Therefore, when the LCL filter resonates, it leads to an increase in electrical stresses on the capacitor, consequently impacting the capacitor's lifetime. A quantitative analysis of this phenomenon will be presented in the following section.

V. Time to Failure and Reliability of LCL Filter Capacitors

The mission profile of the PV inverter system is determined by SI and ambient temperature. However, the electrical stresses on the capacitors, as depicted in Fig. 3, remain unaffected by SI. Thermal stress is recognized as the most critical stressor impacting capacitor reliability [27]. According to the electrical stresses imposed on the filter capacitors with and without the resonant currents, the power loss and thermal behavior of the capacitors during operation are investigated in order to evaluate their lifetime. Specifically, the losses and thermal behavior can be determined through deterministic calculations, while the reliability of the capacitors can be assessed from a probabilistic perspective.

A. Reliability Evaluation Process

In this article, the lifetimes of capacitors are assessed for systems with and without resonant currents, following the flowchart depicted in Fig. 13. Different voltage stresses and current harmonic components can be evaluated through PV and converter modeling, where a current control loop with a damping method is applied in the converter model. When the damping method fails,

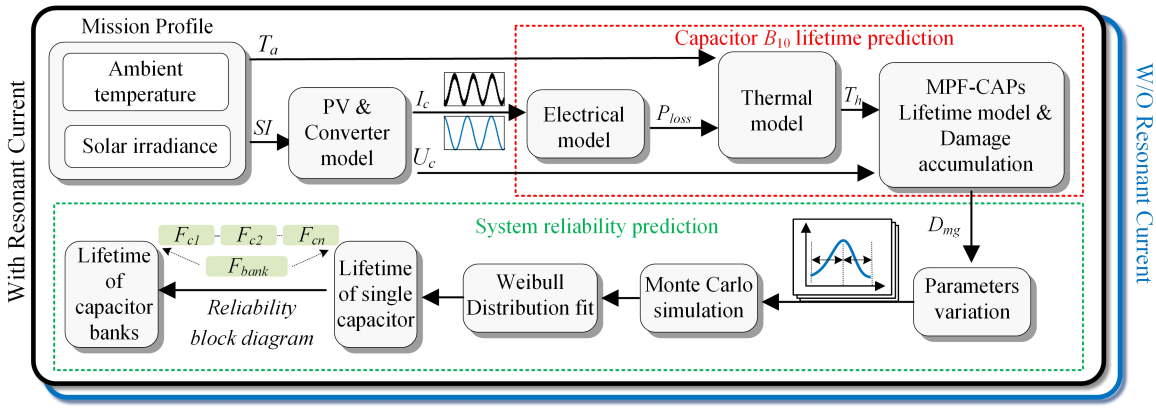

Fig. 13. Flowchart to evaluate reliability from single capacitor to capacitor bank.

the resulting resonant currents lead to variability in the electrical parameters of the module output. Subsequently, dielectric loss and Joule loss dissipation are calculated using the electrical model. The hotspot temperature T_h of the capacitor is derived from the ambient temperature T_a and the capacitor's power loss. The annual damage of the capacitor can be evaluated by the lifetime and damage accumulation models with the voltage stresses and hotspot temperature obtained from the converter model. It is worthwhile to mention that the lifetime in the block diagram is defined as the B_{10} lifetime. Typically, in practical scenarios, variations in component parameters and lifetime models influence the distribution of the probability of failure. Therefore, a Monte Carlo simulation with a large population of samples is calculated and the probability density function (pdf) of a single capacitor is derived through Weibull distribution fitting. Finally, the lifetime of the capacitor bank is obtained through a reliability block diagram, which quantitatively compares the impact of resonant currents on the lifetime.

B. Reliability Analysis of Capacitors

Film capacitors are commonly chosen as filter capacitors to mitigate PWM harmonics between the power converter and the grid. The reliability evaluation of film capacitors includes three steps, outlined as follows. Three capacitor bank configurations described in Section II are selected as examples.

1) Electrothermal Model Analysis: The heat generated by a capacitor primarily comes from power loss, which is closely related to the ESR, ripple current, and frequency of the capacitor [34]. The power loss can be expressed as follows:

$$P_{\text{loss}} = \sum_n \left[\text{ESR} \times I_{\text{rms}}^2(f_n) + \frac{\tan\delta}{\omega_n C} \times I_{\text{rms}}^2(f_n) \right] \quad (12)$$

where ESR and $I_{\text{rms}}(f_n)$ represent the ESR of the capacitor and the root mean square (rms) value of the ripple current at frequency f_n, respectively. The variables n and δ correspond to the harmonic order and dissipation factor, respectively. It should be noted that the ESR curve of a capacitor is not constant and varies with the frequency. Consequently, when assessing the impact of harmonics on the capacitor's hotspot temperature, the dominant harmonic frequencies must be converted to the measured values in the capacitor manufacturer's datasheet [3]. However, LCL filters use polypropylene film capacitors, which exhibit an ESR variation of less than 2% within a temperature range of 0–100° [34]. Therefore, the effect of ESR degradation is ignored in this article.

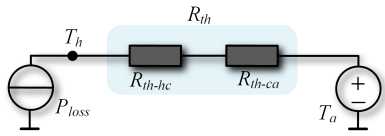

Fig. 14. Simplified thermal model of MPF-CAPs.

Thermal stress is a critical factor for capacitor failure, which can be quantified by the hotspot temperature T_h of the capacitor. Based on the mathematical model, taking the loading transient as an example, the hotspot temperature T_h of MPF-CAPs is affected by the power loss P_{loss} [4] and ambient temperature T_a, as follows:

$$T_h = \triangle T + T_a = P_{\text{loss}} R_{th} + T_a \quad (13)$$

where Rth is the equivalent thermal resistance from the hotspot to the environment, as shown in Fig. 14. It consists of two parts: heat transfer from the hotspot to the case ($R_{\text{th-hc}}$) and heat transfer from the case to the ambient ($R_{\text{th-ca}}$) [18].

By integrating mission profiles, the hotspot temperature of each capacitor can be evaluated through thermal modeling. Fig. 15 displays the hotspot temperature T_h for different capacitors and compares scenarios with and without resonant current. Notably, in the case of the damping method failure, the hotspot temperature of each capacitor is always higher than those observed in the without resonant current case. Specifically, the 15 μF capacitor exhibited the highest hotspot temperature during system oscillations, which is 13.3° higher than the condition without resonant current condition. This temperature variation is primarily due to the significant increase in electrothermal stress on a single 15 μF capacitor when the damping method is ineffective in suppressing resonance, potentially leading to the failure of the film capacitor.

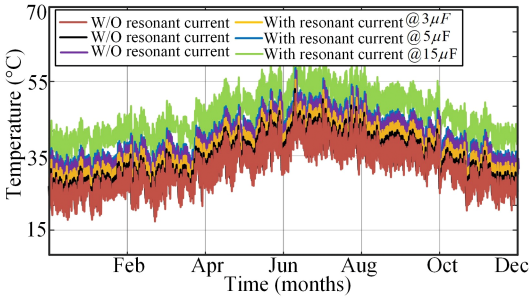

Fig. 15. Temperature profiles for different capacitors with and without resonant currents.

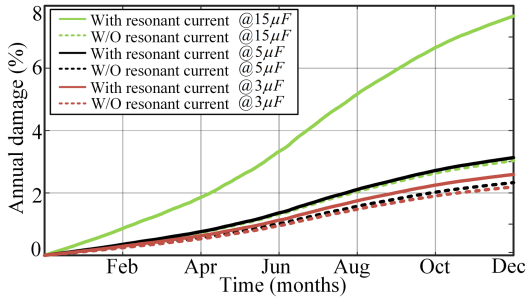

Fig. 16. Accumulated damage for different capacitors with and without resonant currents.

TABLE II
KEY PARAMETERS RELATED TO LIFETIME OF MPF-CAPS

Parameters	15 μF	5 μF	3 μF
Rated voltage V_0 (V)	330	330	330
Rated temperature T_0 (°C)	70	70	70
ESR (mΩ)	3.9	5.2	7.3
Thermal resistance R_{th} (°C/W)	16.5	20.5	23.5
Voltage stress exponent n_2	0.012	0.012	0.012
Dissipation factor $\tan\delta$	6e-4	10e-4	10e-4
Rated lifetime L_0 (hour)	30 000	30 000	30 000

2) Lifetime and Accumulated Damage Evaluation: A widely used capacitor lifetime model [3], [4] with the relationship between hotspot temperature and voltage can be expressed as follows:

$$L_x = L_0 \times 2^{\frac{T_0 - T_h}{10}} \times (V_x/V_0)^{-n_2} \tag{14}$$

where L_0, V_0, and T_0 denote the rated lifetime, rated voltage, and rated temperature, respectively. L_x, V_x, T_h, and n_2 represent the calculated lifetime, capacitor operation voltage, hotspot temperature, and voltage stress exponent, respectively. Table II provides key parameters of the capacitors used in the lifetime evaluation. Furthermore, the capacitor damage accumulated according to Miner's rule can also be determined as follows:

$$D_{\text{mg}} = \sum_{x=1}^{n} \frac{l_x}{L_x} \tag{15}$$

where l_x represents the operation time. Considering the system's long-term operation, the accumulated damage can be converted to capacitance losses [35]. Existing studies have demonstrated that the end of an MPF-CAPs lifetime can be defined as a 5% loss of its initial capacitance [2]. Nevertheless, the capacitance of polypropylene film capacitors has a very weak temperature dependence (0.023%/°C) [27], which means that capacitance degradation has a negligible effect on lifetime prediction.

Based on the mission profile, the annual damage for the different types of capacitors can be calculated as shown in Fig. 16. It is evident that the 3 μF capacitor, when utilizing the damping method, exhibits relatively low annual damage compared to other capacitors. Moreover, 3 μF capacitor at the failure of the damping method has a 0.4% higher annual damage than its damped counterpart. It is clearly observed that the 15 μF capacitor with resonant current has a maximum annual damage

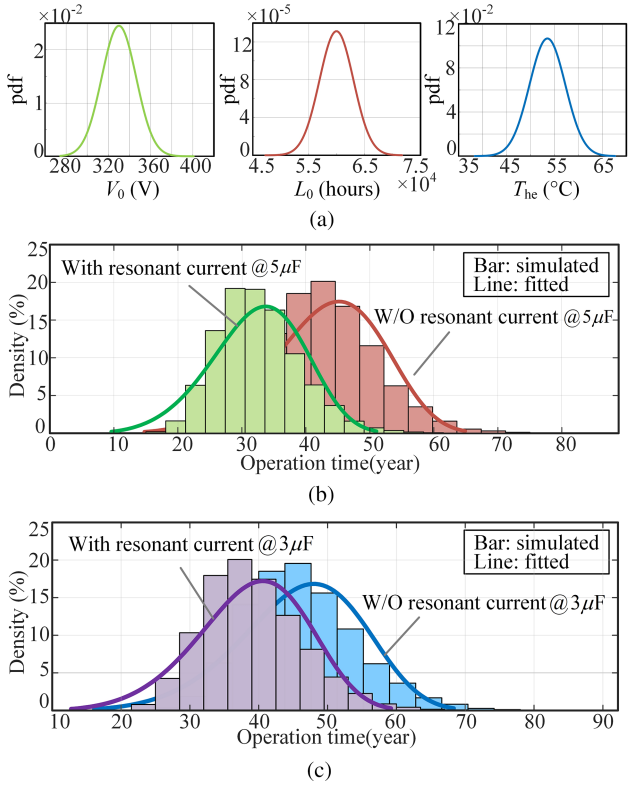

Fig. 17. (a) PDFs of the parameters for capacitor. (b) Histogram of years to failure of 5 μF capacitor with and without resonant currents. (c) Histogram of years to failure of 3 μF capacitor with and without resonant currents.

of 7.6%, as corroborated by the maximum hotspot temperature shown in Fig. 15. However, the damping method can substantially reduce its annual damage to 3.04%. The greatest annual damage to the capacitor is attributed to the largest current stress in this mode. In addition, the current harmonics at the LCL resonant frequency are concentrated on an individual capacitor, leading to increased thermal stress. These factors collectively contribute to a reduced B_{10} lifetime of 15 μF capacitor.

3) Reliability Analysis of Capacitor Banks: To address the uncertainty due to variations in capacitor lifetime models and parameters, a statistical approach based on Monte Carlo simulation is employed in the evaluation process. Assuming that all parameters obey a normal pdf distribution, their sample numbers

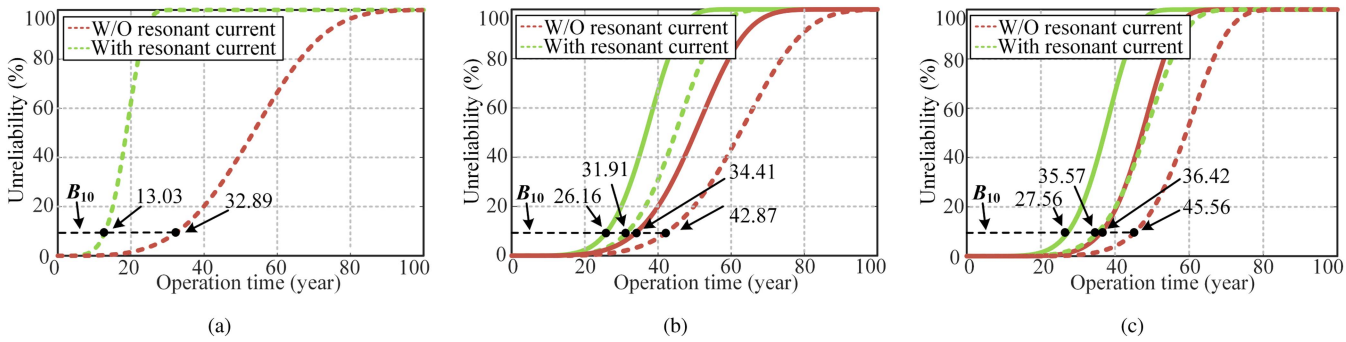

Fig. 18. Unreliability curves for different capacitor bank configurations (solid line: capacitor bank, dotted line: single capacitor). (a) 15 μF capacitor with and without resonant currents. (b) 5 μF capacitor bank with and without resonant currents. (c) 3 μF capacitor bank with and without resonant currents.

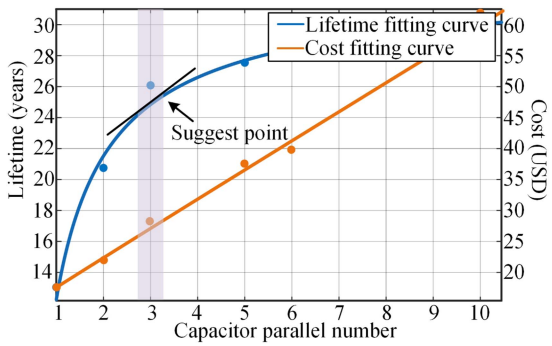

Fig. 19. Lifetime and cost performance of capacitor banks with different parallel numbers.

affect the accuracy of the distribution [8]. Hence, Fig. 17(a) illustrates the selection of 10 000 samples, each of which represents a 5% variation in the chosen parameters [4]. Within these samples, T_{he} corresponds to the calculated equivalent hotspot temperature derived from the D_{mg} [4]. Typically, the histograms of years to failure, as depicted in Fig. 17(b) and (c) can be fitted with the Weibull distribution [10], i.e.,

$$f(t) = (\beta/\eta) \cdot (t/\eta)^{\beta-1} \cdot e^{-\left(\frac{t}{\eta}\right)^{\beta}} \tag{16}$$

$$F(t) = \int f(t)dt = 1 - e^{-\left(\frac{t}{\eta}\right)^{\beta}} \tag{17}$$

where $F(t)$ and $f(t)$, respectively, represent the unreliability function and the pdf of the Weibull distribution, and the value of $F(t)$ belongs to 0–1. β denotes the shape parameter, and η denotes the scale parameter. In the reliability block diagram, all capacitors are connected in series, i.e., the failure of any capacitor will result in the failure of the whole capacitor bank. Then, the capacitor bank failure is represented as (18), where $F_i(t)$ represents the failure function for a single capacitor

$$F_{\text{bank}}(t) = 1 - \prod \left(1 - F_i(t)\right). \tag{18}$$

It is worth noting that the Weibull shape parameters remain constant for the same failure mode [27]. To further assess the reliability of the capacitor bank, the Monte Carlo simulation values can be utilized to derive the Weibull distribution of the capacitor bank. As shown in Fig. 18, a single 15 μF capacitor with system instability exhibits a B_{10} lifetime of only 13.03 years. In contrast, the lifetime of the damping method when operating effectively exceeds 30 years, meeting the designed lifetime of the home PV system. Regarding 5 and 3 μF capacitor banks, it is apparent that the resonant current significantly impacts the lifetime when the damping method fails. The B_{10} lifetimes of the 5 μF capacitor bank are 26.16 and 34.41 years, respectively, with the LCL resonant current reducing the lifetime by about 23.97%. Similarly, The B_{10} lifetimes of 3 μF capacitor bank are 27.56 and 36.42 years, respectively. A case of system resonance results in a 24.32% reduction in the lifetime of the 3 μF capacitor bank. Since 15 μF capacitor is not connected in parallel, according to Fig. 18(b) and (c), it can be seen that the lifetime of a single capacitor surpasses the lifetime of the capacitor bank in any operation mode, with a reduction ranging from 18% to 22%.

In applications where a single capacitor is insufficient, it is common to connect multiple capacitors in series or parallel to create a bank that meets the capacitance and voltage rating requirements. In this study, various types of capacitors are combined to maintain a constant resonant frequency and achieve a total capacitance of 15 μF. Considering constraints related to lifetime, cost, and the number of capacitors, Fig. 19 illustrates the performance space of different capacitor banks. The cost of a capacitor is directly proportional to its energy storage, represented by the equation $E_c = \frac{1}{2}CV^2$ [36], where C and V denote the rated capacitance and voltage, respectively. Consequently, the fitted curve exhibits a linear relationship with the number of capacitors. As the number of capacitors increases, the lifetime of the capacitor bank extends, but it sacrifices its volume and cost at the same time. By analyzing the fitted curve for the cases in this article, it is recommended to parallel three film capacitors. This point represents the tangent at the maximum slope of the curve. Beyond this threshold, the rate of lifetime improvement slows down, and the cost of the capacitor bank increases significantly. Table III lists the cost and lifetime of the three capacitor configurations used in this article. The maximum slope point with 3 $\times$ 5 μF in parallel is the recommended solution, which reduces the cost by 36.3% compared with the solution with 5 $\times$ 3 μF in parallel, with only a 5% decrease in lifetime. Consequently, this configuration achieves a great balance between cost and reliability.

TABLE III
COMPARISON OF LIFETIME AND COSTS IN EACH CONFIGURATION

Parameters	15 μF	5 μF	3 μF
Cost (USD)	17.38	9.72×3	7.95×5
Average lifetime cost (USD/year)	1.33	1.12	1.44

VI. CONCLUSION

This article presents a comprehensive approach to assessing the reliability of LCL–filtered capacitor banks used in PV systems. Initially, an analytical model is introduced to obtain capacitor currents with resonances. The impact of resonant currents on capacitor reliability is quantitatively assessed through detailed modeling of the capacitors' electrical, thermal, and physical characteristics, along with lifetime prediction techniques. In addition, a comparative analysis of average lifetime costs is conducted to optimize economic performance from a reliability perspective. From this case study, the following conclusions can be drawn.

1) Capacitor currents containing resonant distributions are obtained using LCL filter impedance characteristics and Fourier series decomposition. This approach ensures that the analysis of filter capacitor electrical stresses is independent from simulation, easy to modify and optimize, and can be extended to other applications with LCL filters.
2) The effects of resonant currents on capacitor reliability are quantified. In cases where the damping method fails, the hotspot temperature of the 15 μF capacitor increases significantly by 13.3°, leading to a substantial reduction in the B_{10} lifetime, from 32.89 (nonresonant) to 13.03 years.
3) The reliability and cost performance of the capacitor bank are influenced by the number of capacitors in parallel. In this case study, it is suggested that using three 5 μF capacitors in parallel at the maximum slope point can reduce costs by 36.3%, with only a minor 5% reduction in lifetime compared to five 3 μF capacitors in parallel.
4) The introduction of the reliability dimension offers a novel perspective on the design of LCL-type PV systems, emphasizing the vulnerability of capacitors in the event of critical oscillations. The factors influencing reliability vary depending on the capacitor configuration, while the tradeoff between cost and reliability needs to be considered.

In practice, integrating reliability into the predesign stage can improve the overall efficiency of the system. Future research could also consider the thermal coupling effects of capacitor banks for a more comprehensive performance evaluation.

REFERENCES

[1] J. Dannehl, M. Liserre, and F. W. Fuchs, "Filter-based active damping of voltage source converters with LCL filter," *IEEE Trans. Ind. Electron.*, vol. 58, no. 8, pp. 3623–3633, Aug. 2011.

[2] H. Wang et al., "Transitioning to physics-of-failure as a reliability driver in power electronics," *IEEE J. Emerg. Sel. Topics Power Electron.*, vol. 2, no. 1, pp. 97–114, Mar. 2014.

[3] D. Zhou, Y. Song, Y. Liu, and F. Blaabjerg, "Mission profile based reliability evaluation of capacitor banks in wind power converters," *IEEE Trans. Power Electron.*, vol. 34, no. 5, pp. 4665–4677, May 2019.

[4] Z. Zhao, D. Zhou, P. Davari, J. Fang, and F. Blaabjerg, "Reliability analysis of capacitors in voltage regulator modules with consecutive load transients," *IEEE Trans. Power Electron.*, vol. 36, no. 3, pp. 2481–2487, Mar. 2021.

[5] B. Yao et al., "Electrothermal stress analysis and lifetime evaluation of DC-link capacitor banks in the railway traction drive system," *IEEE J. Emerg. Sel. Topics Power Electron.*, vol. 9, no. 4, pp. 4269–4284, Aug. 2021.

[6] Life expectancy model v2.0. KEMET corp., Fort Lauderdale, FL, USA, 2021. [Online]. Available: https://ksim3.kemet.com/film-lifetime

[7] Polypropylene-phb-rhb. Icel S.r.l. Corp., Castellanza, Italy, 2022. [Online]. Available: https://www.icel.it/docs/4022/polypropylene_phb_rhb_2ae5325f58.pdf

[8] H. Wang and F. Blaabjerg, "Reliability of capacitors for DC-link applications in power electronic converters—An overview," *IEEE Trans. Ind. Appl.*, vol. 50, no. 5, pp. 3569–3578, Sep./Oct. 2014.

[9] D. Zhou and F. Blaabjerg, "Converter-level reliability of wind turbine with low sample rate mission profile," *IEEE Trans. Ind. Appl.*, vol. 56, no. 3, pp. 2938–2944, May/Jun. 2020.

[10] D. Zhou, H. Wang, and F. Blaabjerg, "Mission profile based system-level reliability analysis of DC/DC converters for a backup power application," *IEEE Trans. Power Electron.*, vol. 33, no. 9, pp. 8030–8039, Sep. 2018.

[11] M. Liserre, F. Blaabjerg, and S. Hansen, "Design and control of an LCL-filter-based three-phase active rectifier," *IEEE Trans. Ind. Appl.*, vol. 41, no. 5, pp. 1281–1291, Sep./Oct. 2005.

[12] W. Yao, Y. Yang, Y. Xu, F. Blaabjerg, S. Liu, and G. Wilson, "Phase reshaping via all-pass filters for robust LCL-filter active damping," *IEEE Trans. Power Electron.*, vol. 35, no. 3, pp. 3114–3126, Mar. 2020.

[13] A. Akhavan, H. R. Mohammadi, J. C. Vasquez, and J. M. Guerrero, "Passivity-based design of plug-and-play current-controlled grid-connected inverters," *IEEE Trans. Power Electron.*, vol. 35, no. 2, pp. 2135–2150, Feb. 2020.

[14] X. Wang, Y. He, D. Pan, H. Zhang, Y. Ma, and X. Ruan, "Harmonic instability of LCL-type grid-connected inverter caused by the pole-zero cancellation: A case study," *IEEE Trans. Ind. Electron.*, vol. 69, no. 11, pp. 11580–11589, Nov. 2022.

[15] X. Wang, F. Blaabjerg, and P. C. Loh, "Grid-current-feedback active damping for LCL resonance in grid-connected voltage-source converters," *IEEE Trans. Power Electron.*, vol. 31, no. 1, pp. 213–223, Jan. 2016.

[16] J. Ye, H. Wang, B. Li, Y. Huang, J. Xu, and A. Shen, "Passivity-based controller design of PCC voltage feedforward active damping for grid-connected inverters," *IEEE Trans. Ind. Electron.*, vol. 71, no. 8, pp. 8752–8762, Aug. 2024.

[17] X. Wang, X. Ruan, S. Liu, and C. K. Tse, "Full feedforward of grid voltage for grid-connected inverter with LCL filter to suppress current distortion due to grid voltage harmonics," *IEEE Trans. Power Electron.*, vol. 25, no. 12, pp. 3119–3127, Dec. 2010.

[18] H. Wang, P. Davari, H. Wang, D. Kumar, F. Zare, and F. Blaabjerg, "Lifetime estimation of DC-link capacitors in adjustable speed drives under grid voltage unbalances," *IEEE Trans. Power Electron.*, vol. 34, no. 5, pp. 4064–4078, May 2019.

[19] H. Jedtberg, M. Langwasser, R. Zhu, G. Buticchi, and M. Liserre, "Impacts of rotor current control targets on DC-link capacitor lifetime in DFIG-based wind turbine during grid voltage unbalance," in *Proc. IEEE Energy Convers. Congr. Expo.*, 2017, pp. 3489–3495.

[20] X. Pei, W. Zhou, and Y. Kang, "Analysis and calculation of DC-link current and voltage ripples for three-phase inverter with unbalanced load," *IEEE Trans. Power Electron.*, vol. 30, no. 10, pp. 5401–5412, Oct. 2015.

[21] Y. He, X. Wang, X. Ruan, D. Pan, and K. Qin, "Hybrid active damping combining capacitor current feedback and point of common coupling voltage feedforward for LCL-type grid-connected inverter," *IEEE Trans. Power Electron.*, vol. 36, no. 2, pp. 2373–2383, Feb. 2021.

[22] L. Harnefors, R. Finger, X. Wang, H. Bai, and F. Blaabjerg, "VSC input-admittance modeling and analysis above the Nyquist frequency for passivity-based stability assessment," *IEEE Trans. Ind. Electron.*, vol. 64, no. 8, pp. 6362–6370, Aug. 2017.

[23] D. Zhou, H. Wang, and F. Blaabjerg, "Reactive power impacts on LCL filter capacitor lifetime in grid-connected inverter," *IEEE Open J. Power Electron.*, vol. 1, pp. 139–148, May 2020.

[24] N. Agarwal, A. Arya, M. W. Ahmad, and S. Anand, "Lifetime monitoring of electrolytic capacitor to maximize earnings from grid-feeding PV system," *IEEE Trans. Ind. Electron.*, vol. 63, no. 11, pp. 7049–7058, Nov. 2016.

[25] D. Pan, X. Ruan, C. Bao, W. Li, and X. Wang, "Capacitor-current-feedback active damping with reduced computation delay for improving robustness of LCL-type grid-connected inverter," *IEEE Trans. Power Electron.*, vol. 29, no. 7, pp. 3414–3427, Jul. 2014.
[26] AC filtering metalized polypropylene film capacitor radial type, Vishay, Malvern, PA, USA, 2022. [Online]. Available: https://www.vishay.com/docs/26077/mkp1847cacfiltering.pdf
[27] Y. Shen, A. Chub, H. Wang, D. Vinnikov, E. Liivik, and F. Blaabjerg, "Wear-out failure analysis of an impedance-source PV microinverter based on system-level electrothermal modeling," *IEEE Trans. Ind. Electron.*, vol. 66, no. 5, pp. 3914–3927, May 2019.
[28] A. Sangwongwanich, Y. Yang, D. Sera, and F. Blaabjerg, "Lifetime evaluation of grid-connected PV inverters considering panel degradation rates and installation sites," *IEEE Trans. Power Electron.*, vol. 33, no. 2, pp. 1225–1236, Feb. 2018.
[29] H. Wang et al., "Lifetime prediction of DC-link capacitors in multiple drives system based on simplified analytical modeling," *IEEE Trans. Power Electron.*, vol. 36, no. 1, pp. 844–860, Jan. 2021.
[30] Y. Wang, X. Wang, F. Blaabjerg, and Z. Chen, "Harmonic instability assessment using state-space modeling and participation analysis in inverter-fed power systems," *IEEE Trans. Ind. Electron.*, vol. 64, no. 1, pp. 806–816, Jan. 2017.
[31] V. Prasad, D. Borojevic, and R. Zhang, "Analysis and comparison of space vector modulation schemes for a four-leg voltage source inverter," in *Proc. IEEE Appl. Power Elect. Conf.*, 1997, pp. 864–871.
[32] D. G. Holmes and T. A. Lipo, *Pulse Width Modulation for Power Converters: Principles and Practice*. Hoboken, NJ, USA: Wiley, 2003.
[33] Y. Tang, W. Yao, P. C. Loh, and F. Blaabjerg, "Design of LCL filters with LCL resonance frequencies beyond the Nyquist frequency for grid-connected converters," *IEEE J. Emerg. Sel. Topics Power Electron.*, vol. 4, no. 1, pp. 3–14, Mar. 2016.
[34] H. Wang, C. Li, G. Zhu, Y. Liu, and H. Wang, "Model-based design and optimization of hybrid DC-link capacitor banks," *IEEE Trans. Power Electron.*, vol. 35, no. 9, pp. 8910–8925, Sep. 2020.
[35] J. Wei, H. Feng, and L. Ran, "Multidimensional design of DC-link for two-stage solid-state transformer cell considering second-order harmonic current distribution," *IEEE Trans. Power Electron.*, vol. 38, no. 8, pp. 10244–10255, Aug. 2023.
[36] R. Burkart and J. W. Kolar, "Component cost models for multi-objective optimizations of switched-mode power converters," in *Proc. IEEE Energy Convers. Congr. Expo.*, 2013, pp. 2139–2146.

Jiacheng Sun (Graduate Student Member, IEEE) received the B.E and M.S. degrees in electrical engineering from the Northwestern Polytechnical University, Shaanxi, China, in 2016 and 2019, respectively. He is currently pursuing the Ph.D. degree with the Northwestern Polytechnical University. From 2021 to 2023, he was a visiting Ph.D. with Aalborg University, Aalborg, Denmark.

His research interests include current control, grid-connected inverters, reliability of power electronics in renewable energy application.

Xinyue Zhang (Member, IEEE) received the B.E and M.S. degrees in electrical engineering from the Northwestern Polytechnical University, Xi'an, China, in 2016 and 2019, respectively. She is currently working toward the Ph.D. degree in power electronics. She was a visiting student with Aalborg University, Aalborg, Denmark, from 2022 to 2023. Her current research interests include the thermal analysis and reliability of power electronic devices.

Wenli Yao (Member, IEEE) received the B.S., M.S., and Ph.D. degrees in electrical engineering from Northwestern Polytechnical University, Xi'an, China, in 2009, 2012, and 2017, respectively. Since May 2019, he has been with Northwestern Polytechnical University, Xi'an, China, as an Associate Professor. His research interests include current control, grid-connected inverter, multi-pulse converter, and power decoupling.

Xiaobin Zhang received the B.S. and M.S degrees in electrical engineering from the School of Automation, Northwestern Polytechnical University, Xi'an, China, in 1983 and 1986, respectively. Since 1986, he has been with the School of Automation, Northwestern Polytechnical University, where he is currently a Professor. His research interests include power electronic control, aircraft power system, multi-pulse converter.

Dao Zhou (Senior Member, IEEE)) received the B.S. from Beijing Jiaotong University, Beijing, China, in 2007, the M.S. from Zhejiang University, Hangzhou, China, in 2010, and the Ph.D. from Aalborg University, Aalborg, Denmark, in 2014, all in electrical engineering. Since 2014, he has been with Department of Energy, Aalborg University, where currently he is an Associate Professor. His research interests include modeling, control, and reliability of power electronics in renewable energy applications. He serves as an Associate Editor for IEEE TRANSACTIONS ON INDUSTRY APPLICATIONS. He received a few IEEE prized paper awards.